Assessment of Acoustic Behavior for Perforate-Over-Large-Cell Liners

Martha C. Brown*, Chelsea Solano†, Jordan R. Kreitzman ‡, Michael G. Jones§
NASA Langley Research Center, Hampton, VA 23681

2023 AIAA AVIATION Forum
12-16 June 2023; San Diego, CA

This study explores the effects of increasing the cell size for large-cell acoustic liners. Tests are conducted in the NASA Langley Grazing Flow Impedance Tube to evaluate liners with increasingly larger cell dimensions (up to 2" x 4" cross-section). Conventional impedance eduction confirms that liners with 2" x 3" cells (or larger) must be evaluated using nonlocally reacting assumptions. In addition, due to the sound propagation within cavities, the liners must be modeled using higher fidelity techniques. Thus, grazing flow duct and acoustic liner are modeled simultaneously using finite element methods. The facesheet is modeled using a transfer impedance, while the rest of the domain is modeled using the convected Helmholtz equation. The acoustic pressures predicted are shown to compare favorably with those measured in the Grazing Flow Impedance Tube.

I. Introduction

Since the first half of the 1950s, acoustic liners have been investigated as a way to lessen aircraft noise.[1] These passive devices are typically installed in the nacelle inlet and aft-bypass duct walls of aircraft to absorb tonal noise (caused by rotor-alone and rotor-stator interaction) and broadband noise (caused by turbulent flow through the nacelle) sources produced by the fan. The aircraft engine bypass ratio has steadily risen to improve propulsive efficiency with the fortunate side effect of lessening jet noise. However, the broadband fan noise component has increased in dominance relative to other noise sources due to increasing the engine bypass ratio.

Nearly all liners employed in modern commercial aircraft nacelles are perforate-over-honeycomb structures. Traditional perforate-over-honeycomb liners have chambers with an effective diameter of 0.375". This ensures only plane waves propagate inside the chamber over the operating frequency range. This chamber diameter also enables the honeycomb core to maintain structural integrity. When the dimensions of the chamber are sufficiently small that the sound propagation is dominated by motion in the direction perpendicular to the facesheet, the liner is classified as locally reacting. However, if the cell diameter is increased, sound may propagate in all directions within the chamber. In this case, the liner is classified as nonlocally reacting. It is of interest to explore the feasibility of employing chambers with larger cross sections for use in nontraditional locations within the aircraft engine nacelle. This will require an improved understanding of the acoustical behavior of liners with larger chamber dimensions.

This paper investigates the effects of increasing the liner cell dimensions beyond the 2" x 2" cell size explored in a previous study[2,3] for the benefit of reducing weight. As the cell dimensions increase, the liner has fewer partitions, which translates into less weight and less bonding adhesive.

*Senior Research Engineer, Research Directorate, Aeroacoustics Branch, martha.c.brown@nasa.gov.
†FSU Graduate Research Assistant and NASA Langley Pathways Intern, chelsea.a.dodge@nasa.gov, AIAA Student Member.
‡Research Engineer, Research Directorate, Structural Acoustics Branch, jordan.r.kreitzman@nasa.gov.
§Senior Research Scientist, Research Directorate, Structural Acoustics Branch, michael.g.jones@nasa.gov, AIAA Associate Fellow.

The previous investigation[2] explored three cell dimensions up to 2" x 2" and four facesheets of various porosities. These samples were tested in the NASA Langley Grazing Flow Impedance Tube (GFIT) with source sound pressure levels of 120 and 140 dB at flow conditions of Mach 0.0 and 0.3. Researchers set the maximum size of 2" x 2" to correspond to the width of the GFIT test section. Results showed that not only was the local-reacting assumption valid at this cell diameter, but also this size had a minimal effect on the acoustic performance of a liner over the frequency range of interest (up to 3.0 kHz). The 2" x 2" cell also exhibited a flatter reactance spectrum, resulting in increased attenuation over a broader frequency range. These preliminary results proved promising to continue the investigation in a more complex acoustic environment (e.g., higher-order modes).

In the subsequent investigation,[3] flow conditions were extended to Mach 0.5 and an additional source sound pressure level of 150 dB was included for GFIT testing. Also, larger liner panels were fabricated and tested in the NASA Langley Curved Duct Test Rig (CDTR), where they were exposed to a controlled complex acoustic environment. Four target modes were tested at two flow conditions (Mach 0.0 and Mach 0.3). Results showed that the cavity size effects were more evident in the presence of higher-order modes but remained sufficiently well contained to suggest that prediction models previously developed for small diameter cells could be successfully applied to account for these differences in core cell sizes. Nevertheless, there were sufficient differences in acoustic performance to warrant further detailed analysis. A follow-on computational study was needed to evaluate these effects further.

Gravagnone et al.[4] also investigated effective cell diameters up to 2" and porous cell walls as nonlocally reacting liners to broaden the attenuation spectrum of a single-layer liner. They used the commercial finite element software COMSOL Multiphysics®[5] to model the insertion loss of their test articles and also to model the sound propagation in a large-diameter chamber. Flow conditions of Mach 0.0, 0.3, and 0.5 were investigated for upstream and downstream sound propagation. The findings showed that a large-diameter cell increases the attenuation bandwidth and that these improvements were unaffected by the facesheet resistance and the direction of sound propagation.

The current paper will explore larger cell dimensions where the local-reacting assumption becomes invalid. Instead of square cells, the shape of the cells will be rectangular based on the GFIT rectangular test section geometry. Core cell sizes up to 2" by 4" were fabricated and tested in the GFIT at sound pressure levels of 120 and 140 dB and flow speeds of Mach 0.0 and 0.3. The goals of this study are to evaluate the acoustic effectiveness (sound absorption) of large-cell liners and to determine the ability of propagation codes to predict the acoustic performance of large-cell liners.

This investigation explores the acoustic behavior of large-cell liners. The paper is organized as follows: in Section II, the paper will give a brief discussion on acoustic liners; in Section III, the paper will describe the liner samples, the GFIT test rig, impedance eduction methodology; Section IV presents the modeling methodology; in Section V, the paper will show comparison of measured and predicted results; followed by Section VI, where there is a review on the highlights of the paper and potential follow-on research opportunities.

II. Acoustic Liner Background

A. Acoustic Impedance

The acoustic impedance is defined as the ratio of the acoustic pressure, p, and the normal component of the acoustic particle velocity, v_N, at the surface of the liner. It is normalized with respect to the characteristic impedance of sound in air, $\rho_0 c_0$ where ρ_0 and c_0 represent the local density and speed of sound in air, respectively. The surface impedance of the liner is comprised of the resistance, θ, and reactance, χ. The equation is listed below:

$$\zeta = \frac{1}{\rho_0 c_0} \frac{p}{v_N} = \theta + i\chi. \tag{1}$$

Locally reacting liners are typically modeled via this impedance boundary condition in propagation codes, allowing one to predict their impact in various applications. However, this boundary condition breaks down when the cell dimensions become sufficiently large. This study seeks to better understand this breakdown.

B. Single Degree of Freedom (SDOF) Liner

The Single Degree-of-Freedom (SDOF) liner (see Fig. 1) has a single-layer sandwich construction with a solid backplate, porous face sheet, and internal partitions, as would be provided by a honeycomb. The facesheet can be a perforate with or without bonded wire mesh. SDOF liners are often referred to as quarter-wavelength resonators, as their acoustic performance (absorption) is most efficient at frequencies for which the wavelength is approximately four times the depth of the core chamber. In addition, these passive devices provide good attenuation for frequencies surrounding this resonance.

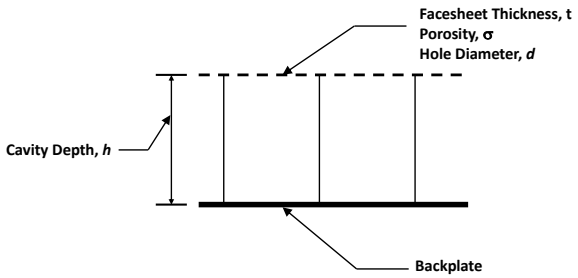

Figure 1: Sketch of SDOF Liner.

III. Experimental Method

A. Evaluation Liners

Each liner used in this study consists of a perforate facesheet, rectangular core chambers, and a rigid back plate. To investigate large-cell liners, the shape of the core cell is now rectangular based on the test section dimensions in the GFIT. Three samples with rectangular core cells were fabricated with a fixed cavity depth, $h = 1.50$", facesheet thickness, $t = 0.030$", perforate hole diameter, $d = 0.040$", and a constant porosity, $\sigma = 0.080$, over each core cell. The width of the partition between each cell is 0.10". Each large-cell sample was 3D printed via stereolithography (SLA). The three large-cell liners have the following cross-sectional dimensions (width x length): (1) 2" x 2" (active liner length: 15.04"); (2) 2" x 3" (active liner length: 15.70"); and (3) 2" x 4" (active liner length: 12.48"). The active liner length is the total axial length of acoustic treatment (as many cells as would fit within the total length of 16"). The leading edge of the active liner length is assumed to start at one-half a partition thickness upstream of the first cell. The trailing edge of the active liner length ends at one-half a partition thickness downstream from the last cell. The other walls in the test section are identified as rigid. The outer dimensions of each sample were 2.49" x 16". Figure 2 is a top view of the three large-cell liners of different sizes. Table 1 shows the dimensions of the cavities, the number of cells, and the active liner length of each sample. The core and facesheet components were designed to be integrated during the SLA printing. However, the core/facesheet integration posed a challenge: keeping a 0.030" thick facesheet from warping during the printing process. Support structures are typically necessary to print parts with overhangs or complex shapes successfully. In this application, support structures kept the facesheet relatively flat over the 2" x 3" and 2" x 4" large cells to minimize sagging in the middle of their respective cells. The support structures were removed once the printing was completed.

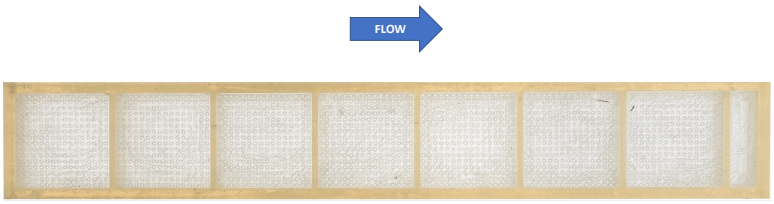

(a) 2” x 2” cross-section large-cell liner, Active Liner Length=15.04”.

(b) 2” x 3” cross-section large-cell liner, Active Liner Length=15.7”.

(c) 2” x 4” cross-section large-cell, Active Liner Length=12.48”.

Figure 2: Top view of GFIT large-cell liners.

Table 1: Dimensions of the large-cell liners.

Cell Cross-Section	Number of Cells	Active Liner Length
2” x 2”	7	15.04”
2” x 3”	5	15.70”
2” x 4”	3	12.48”

B. Grazing Flow Impedance Tube (GFIT)

The GFIT (see Fig. 3) is used to evaluate the acoustic performance of each liner. The GFIT has a cross-sectional geometry of 2.00” wide x 2.50” high, such that higher-order modes in the horizontal and vertical dimensions cut on at different frequencies. It allows evaluation of acoustic liners with lengths from 2.00” to 24.00”. The surface of the test liner forms a portion of the upper wall of the flow duct. For this investigation, the source section consists of twelve acoustic drivers mounted upstream of the test section. The source location is the $x = 0$” plane. The drivers are stepped between 400 and 3000 Hz in increments of 100 Hz while the source amplitude is maintained to the same accuracy (within 0.5 dB of its target sound pressure level). Source amplitude levels of 120 and 140 dB were tested in this study. In this diagram, the GFIT is configured in aft mode, where the dominant sound propagation is moving in the same direction as the flow. These tests were conducted at flow speeds of Mach 0.0 and 0.3.

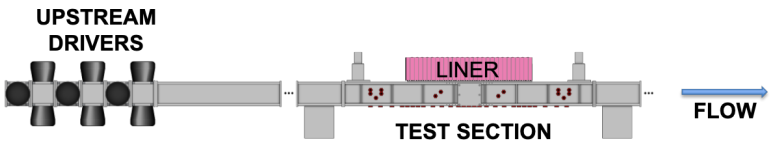

Figure 3: Artist rendition of GFIT.

Fifty-three flush-mounted microphones located in the lower wall (opposite the liner) are used to measure the acoustic pressure field over the axial length of the test section, $L = 40$" (see Fig. 4). The leading edge of the liner (designated by L_1) is 8.25" from the x=0" plane, and the trailing edge of the liner is represented by L_2. A cross-spectrum signal extraction method[6] is used to determine the amplitudes and phases at each of the microphone locations relative to the amplitude and phase at the reference microphone location.

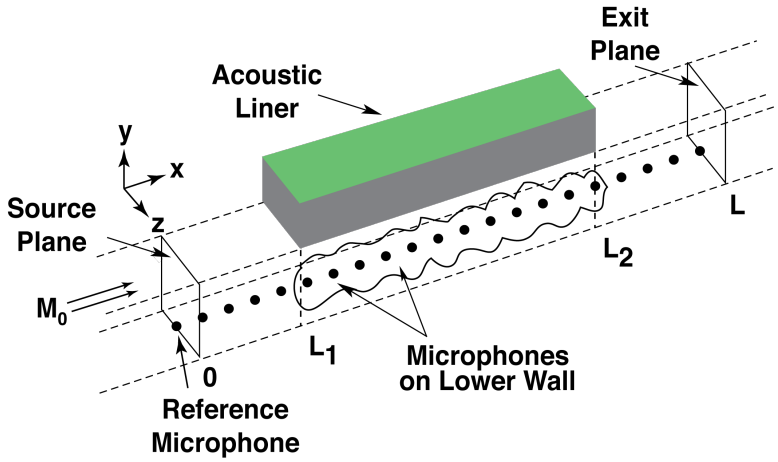

Figure 4: Schematic diagram of GFIT test section.

C. Impedance Eduction Method

Each liner was evaluated using a conventional impedance eduction approach,[7,8] assuming they were locally reacting. The significant divergence of these educed impedances from those educed for liners with smaller cell dimensions indicates that these liners should instead be evaluated as nonlocally reacting liners. Figure 5 provides the impedance spectra for the 2" x 2" and 2" x 3" large-cell liners with a source SPL of 120 dB at Mach 0.0. Although there are some anomalies, the 2" x 2" large-cell liner impedance spectra are relatively smooth. In contrast, the impedance spectra educed with the 2" x 3" large-cell liner are significantly distorted. These distortions, also observed for the 2" x 4" large-cell liner, confirm the need for evaluation using nonlocally reacting assumptions.

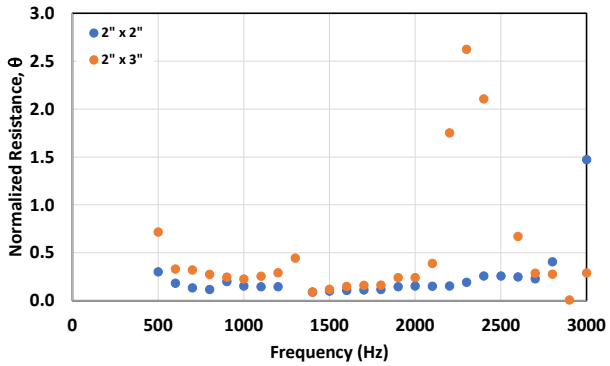

(a) Normalized Resistance.

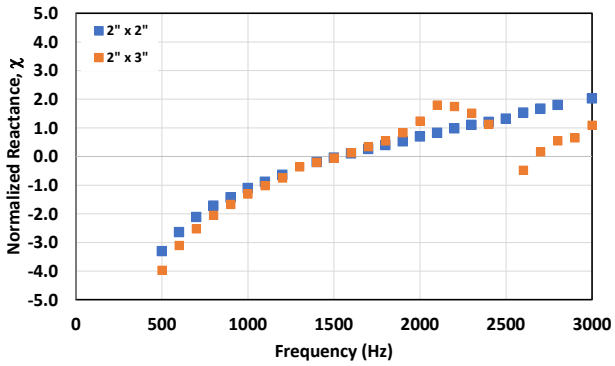

(b) Normalized Reactance.

Figure 5: Comparison of impedance spectra between 2" x 2" and 2" x 3" large-cell liners at Mach 0, 120 dB.

IV. Finite Element Model of a Large-Cell Liner

Locally reacting liners can be modeled as an impedance boundary condition in conventional propagation codes such as COMSOL Multiphysics® and ACTRAN/TM.[9] However, for nonlocally reacting liners, sound transmission within the cells of the liner and through the waveguide must also be considered. Therefore, the facesheet is modeled with a transfer impedance boundary condition and the remaining domain with the convected Helmholtz equation where the equations are solved using finite element analysis. Two commercially available finite element codes, COMSOL Multiphysics® and ACTRAN/TM,[9] were considered for these analyses. Three options were considered for the determination of the facesheet transfer impedance. The transfer impedance was either empirically extracted from the experimental results of the 2" x 2" impedance eduction or modeled using the Two-Parameter[10] or Goodrich[11] models. As expected, both propagation codes provided virtually identical results. Thus, both COMSOL Multiphysics® and ACTRAN/TM were used in parallel during the analysis process.

A. Geometry

Figure 6 illustrates the 3D modeling domain of each of the three samples with respect to the GFIT test section. The 3D modeling domain mimics the 40" long test section that has a height of 2.50" and width of 2.00". The sample is placed 8.25" downstream of the domain inlet. The modeling domains for the large cells of cross-sectional dimensions 2" x 2", 2" x 3", and 2" x 4" are illustrated in Figs. 6a, 6b and 6c, respectively. The facesheet is the light blue sheet between the duct and the cavities. Each figure highlights the source plane (highlighted in green) at $x = 0$" and the termination plane (highlighted in red) at $x = 40$". Dominant sound propagation and flow travels from left to right in each figure.

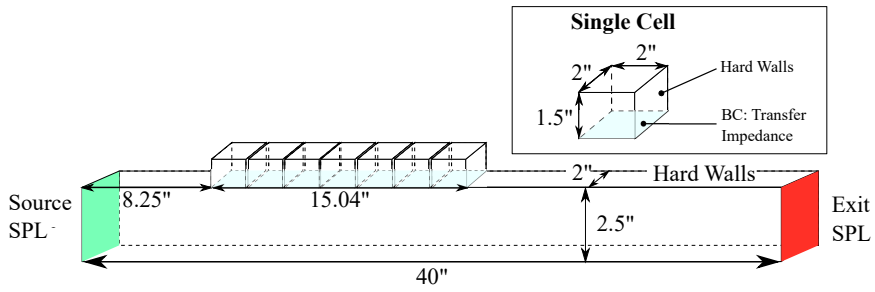

(a) Computational domain with 2" x 2" cells.

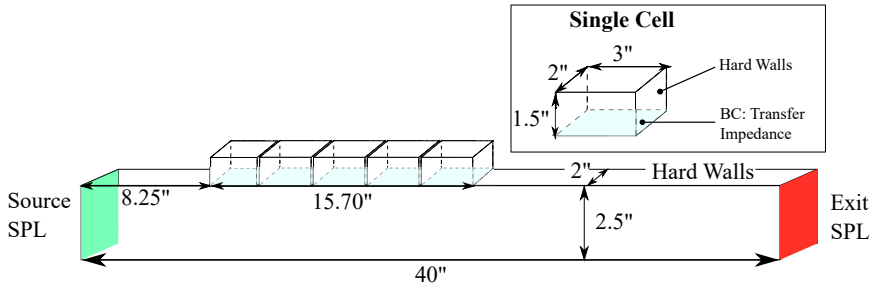

(b) Computational domain with 2" x 3" cells.

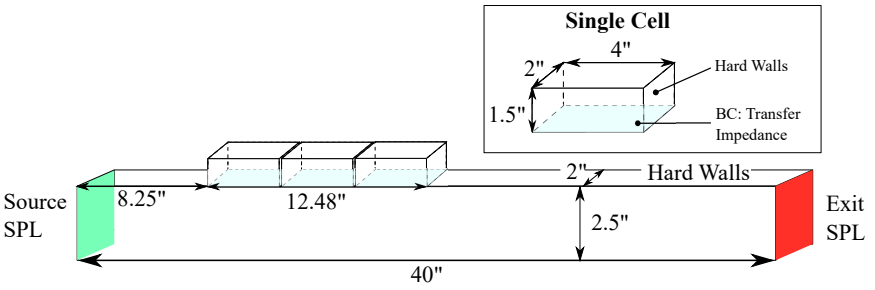

(c) Computational domain with 2" x 4" cells.

Figure 6: 3D schematic of the modeling domain for the large-cell samples in this study.

B. Governing Equation

A few assumptions are made to simplify the problem and governing equations. First, the GFIT is assumed to have inviscid and irrotational flow, or potential flow. The flow profile is assumed uniform across the 2.0" x 2.5" duct, where the average Mach number (M) is either 0.00 for the no flow case or 0.237 for the flow case. The reader should note that the average Mach number for invicid flow is different from the centerline Mach number of 0.3 measured in the GFIT. The uniform flow profile assumption is believed reasonable for the work here, where the average flow profiles for three test liners are shown in Jones et al.[12] The simulation is performed in the frequency domain and is assumed to have a time-harmonic solution, simplifying the problem to be time-independent. Finally, nonlinear terms are neglected such that the governing equation used is the convected Helmholtz equation or

$$-\frac{\rho_0}{c_0^2} i\omega \left(i\omega\phi + \mathbf{V}\cdot\nabla\phi\right) + \nabla\cdot\left[\rho_0\nabla\phi - \frac{\rho_0}{c_0^2}\left(i\omega\phi + \mathbf{V}\cdot\nabla\phi\right)\mathbf{V}\right] = 0, \tag{2}$$

where ϕ is the velocity potential, $\omega = 2\pi f$ is the radian frequency, and $\mathbf{V} = [Mc_0, 0, 0]$ is the mean background velocity vector. The mean background velocity is assumed to be uniform down the duct. The density, speed of sound, and Mach number are all calculated directly from what was measured during the test. The acoustic pressure may be solved for in terms of the velocity potential

$$p = -\rho_0(i\omega\phi + \mathbf{V} \cdot \nabla\phi), \tag{3}$$

allowing for comparisons to the acoustic pressure measured in experiments (i.e., GFIT). Generated meshes were sufficiently resolved to frequencies above the highest frequencies of interest.

C. Boundary Conditions

All boundaries in the domain are acoustically rigid except for the inlet (green in Fig. 6), exit (red in Fig. 6), and facesheet (light blue in Fig. 6). The inlet and exit planes are set to the measured acoustic pressures and are input as a function of magnitude and phase

$$p = Pe^{i\psi}, \tag{4}$$

where P is the magnitude (Pa) and ψ is the phase (rad). The acoustic pressures at the inlet and exit are then converted to potential (ϕ) for use in the simulation. This is either directly calculated using Eq. 3 for the no flow case ($\mathbf{V}$=0), or iteratively solved until the computed pressure matches the desired value. If experimental data are not available, an anechoic termination can be used in the exit plane of the duct.

The remaining boundary condition is an interior impedance condition for the facesheet. This transfer impedance is equal to the pressure drop across the facesheet divided by the normal component of the particle velocity. When mean flow is included, the Myers boundary condition is used in conjunction with the impedance to account for the infinitely thin boundary layer of the flow field.[13] Three transfer impedance models were evaluated for use in the finite element model (FEM): 1) empirically extracted from experiments, 2) the Goodrich model,[11] and 3) the Two-Parameter Model.[10] For the empirical case, the transfer impedance was extracted from measured data for the 2" x 2" case. The cavity impedance was subtracted from the experimentally educed impedance, where the experimental impedance was calculated based on the method outlined in Watson and Jones.[14] This yields a facesheet transfer impedance, ζ_{FS} equal to

$$\zeta_{FS} = \zeta_{exp} - (-cot(kh)) = \zeta_{exp} + cot(kh), \tag{5}$$

where ζ_{exp} is the experimentally educed normalized specific acoustic impedance, $k = \omega/c$ is the wave number, and h is the cavity depth (1.50").

To compare the facesheet transfer impedance models, simulations are run for the 2" x 2" cross-section cavity at Mach 0 and an SPL at the liner leading edge of approximately 120 dB. The SPL profile for 1500 Hz is plotted in Fig. 7, where the black circles are the experimentally measured SPLs, the blue line uses the empirical transfer impedance, the red line uses the Goodrich model, and the grey dashed line uses the Two-Parameter Model. The results using the empirical transfer impedance have the best alignment out of the three cases followed by Goodrich, and then the Two-Parameter Model. The Two-Parameter transfer impedance has poor comparison at this frequency while the Goodrich model has fair comparison, aligning well with the empirical model. As the user may not always have access to measured data from which to determine a transfer impedance, the authors decided not to rely on experimental results for the remainder of this study. Instead, the Goodrich model is used.

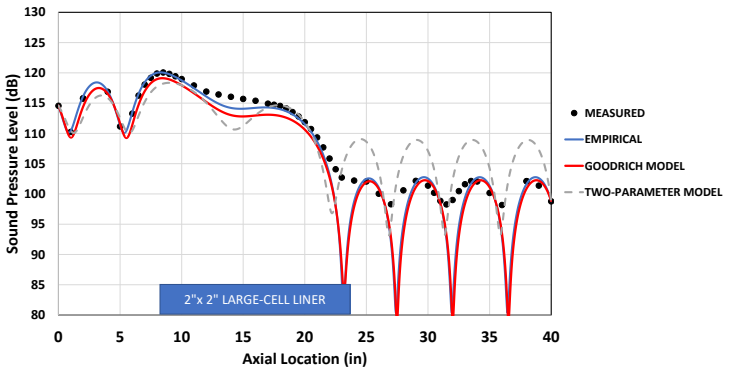

Figure 7: SPL profile over length in the GFIT duct for the three facesheet impedance models evaluated for the 2" x 2" large-cell liner at 1500 Hz, Mach 0, 120 dB.

V. Results and Discussion

As stated earlier, the goals of this study are to evaluate the acoustic effectiveness (sound absorption) of large-cell liners and to determine the ability of propagation codes to predict the acoustic performance of large-cell liners.

Figures 8 and 9 address the first goal by comparing the Sound Pressure Level (SPL) profiles for each large-cell liner. The SPL profiles are provided at frequencies below, near, and above resonance for the 2" x 2" large-cell liner. The axial length of 40" is the length of the GFIT test section. Figure 8 compares the SPL profiles of the 2" x 2", 2" x 3" and 2" x 4" large-cell liners over the length of the test section at Mach 0, 120 dB. Results at 140 dB exhibited similar performance, therefore, the results are not presented in this paper. Each plot illustrates the size of the respective large-cell liners so the reader can view the locations of the leading and trailing edges with respect to the test section. Figures 8a and 8c show the SPL profiles away from resonance, and Fig. 8b illustrates the SPL profiles near resonance. These plots show that at 1500 Hz for a no-flow condition, the 2" x 3" and the 2" x 4" large-cell liner core samples exhibit sound attenuation over the length of the liner. At the upper and lower frequencies, the standing wave pattern becomes more pronounced for the 2" x 4" large-cell liner (i.e., large differences between the maximum and minimum SPL levels), but the liner still absorbs sound. Indeed, although these larger cells cause the locally reacting impedance assumption to break down, they nevertheless produce good sound absorption. Figure 9 shows the corresponding results for the Mach 0.3, 120 dB test condition. Again, the liners with larger cells are observed to provide attenuation similar to that observed for the 2" x 2" large-cell liner. The reader should note that the three samples have different active liner lengths, so each sample should not be compared on a one-on-one basis.

Section IV discussed issues related to modeling the large liner cells and including the transfer impedance in the propagation calculation to define the aeroacoustic field throughout the duct. For this modeling method to be successful, the predicted results will compare well with the measured results. Figures. 10 through 13 address the second goal of this study. ACTRAN/TM was used to generate the predictions presented in Figs. 10 and 11. Figure 10 compares the SPL axial profiles of the measured and predicted results for each large-cell core liner at their respective frequencies for the no-flow condition at 120 dB. Each figure illustrates the location of their respective liner with respect to the test section. Results show that not only does the prediction compare well for the 2" x 2" large-cell liner, but also the predictions compare well for large-cell liners of 2" x 3" and 2" x 4" with the facesheet transfer impedance for the 2" x 2" applied.

Figure 11 compares the SPL axial profiles of the measured and predicted results for each large-cell liner at their respective frequencies for the Mach 0.3 flow condition at 120 dB. Again, predicted results compare well with measured results, and for most of the cases the prediction captured the impedance discontinuity at the trailing edge of the large-cell liner. The comparison degrades somewhat for test conditions where the attenuation is significant, but nevertheless remains quite favorable. Together, Figs. 10 and 11 clearly

demonstrate the efficacy of the use of a Goodrich model-based transfer impedance for this analysis.

COMSOL was used to generate the predictions in Figs. 12 and 13. Figure 12 presents the real component of acoustic pressure throughout the liner and duct for the 2" x 2" and 2" x 3" large-cell liners, respectively. The test condition is Mach 0.0, with a source SPL of 120 dB at 1000 Hz. Observe that the pressure within each 2" x 2" cell is uniform, whereas there is a slight axial gradient within the 2" x 3" cells. This pressure gradient indicates the transition from a locally reacting configuration to a nonlocally reacting configuration, i.e., the sound is allowed to transmit axially within the cell. This effect is more evident in Fig. 13, where the frequency has been increased to 2000 Hz. There is strong axial transmission within the 2" x 3" cells at this frequency, while the sound field within the 2" x 2" cells remains reasonably uniform.

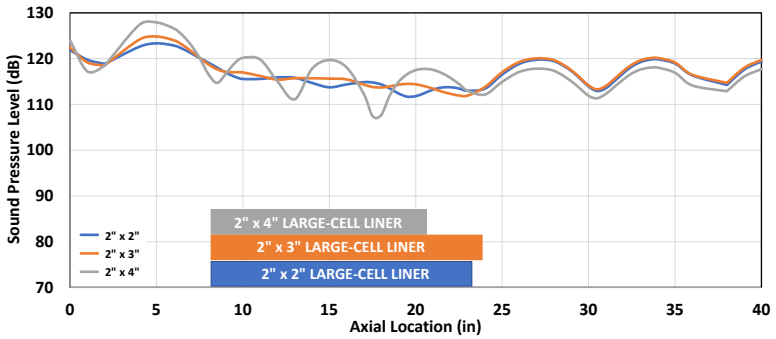

(a) SPL profile at 1000 Hz.

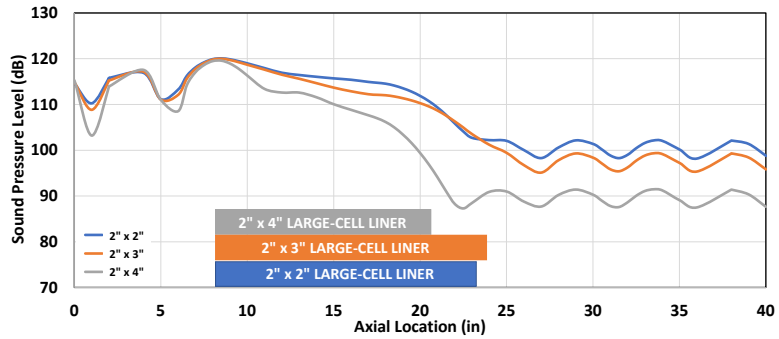

(b) SPL profile at 1500 Hz.

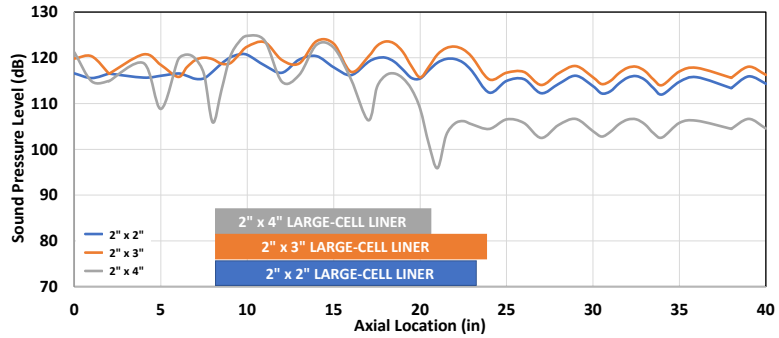

(c) SPL profile at 2000 Hz.

Figure 8: Comparison of measured SPL axial profiles for large-cell liners at Mach 0, 120 dB.

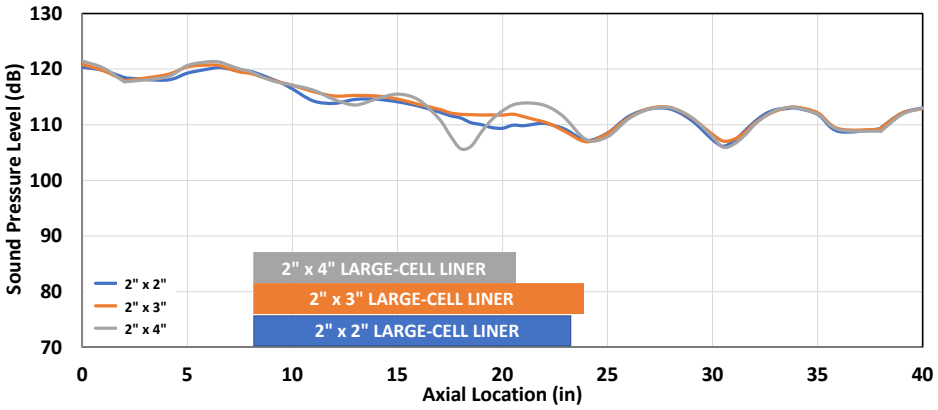

(a) SPL profile at 1000 Hz.

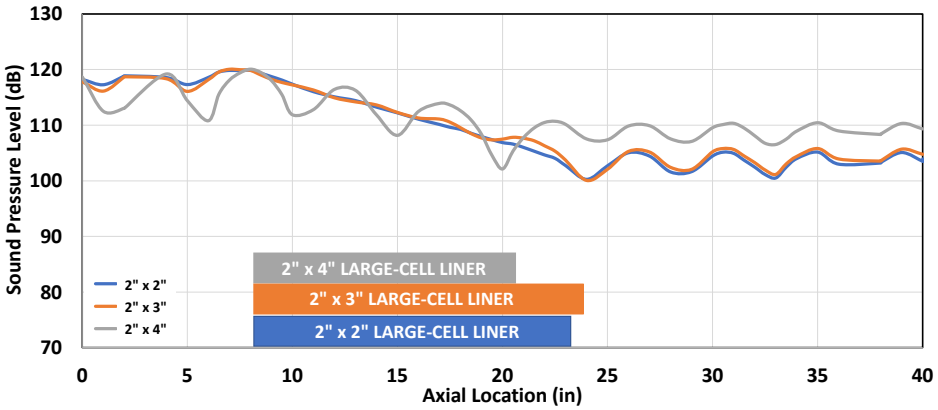

(b) SPL profile at 1500 Hz.

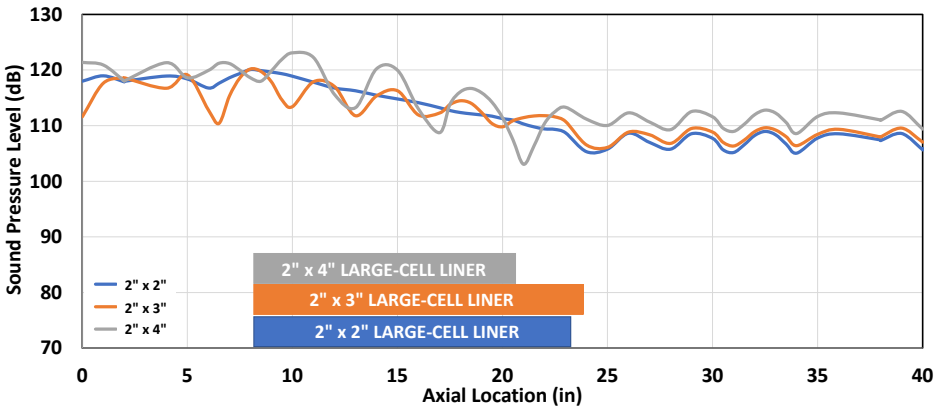

(c) SPL profile at 2000 Hz.

Figure 9: Comparison of measured SPL axial profiles for large-cell liners at Mach 0.3, 120 dB.

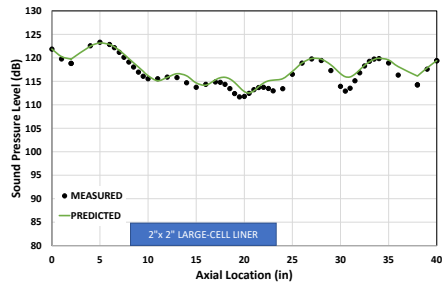

(a) 2” x 2” large-cell liner, 1000 Hz.

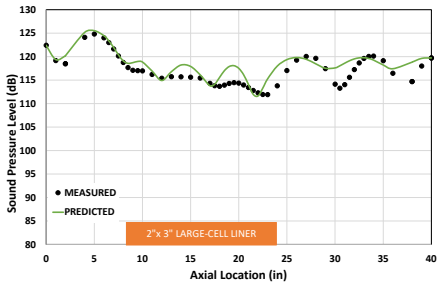

(b) 2” x 3” large-cell liner, 1000 Hz.

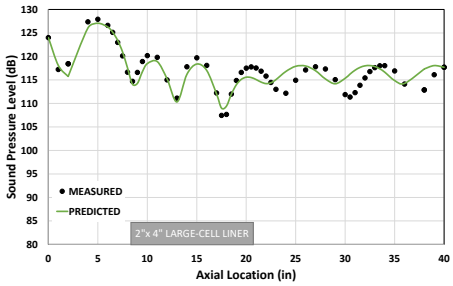

(c) 2” x 4” large-cell liner, 1000 Hz.

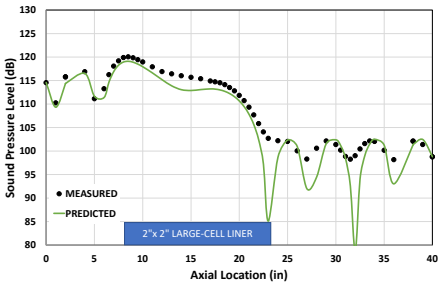

(d) 2” x 2” large-cell liner, 1500 Hz.

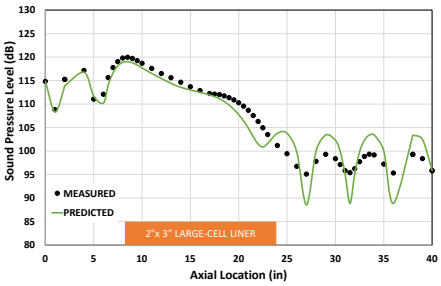

(e) 2” x 3” large-cell liner, 1500 Hz.

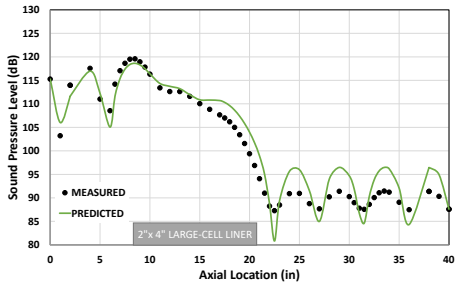

(f) 2” x 4” large-cell liner, 1500 Hz.

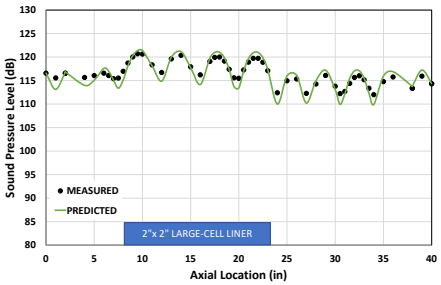

(g) 2” x 2” large-cell liner, 2000 Hz.

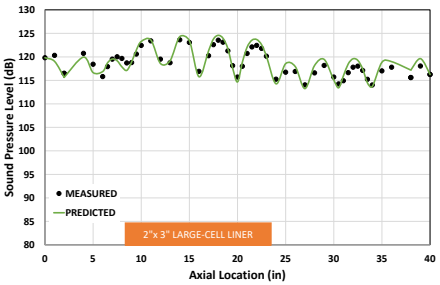

(h) 2” x 3” large-cell liner, 2000 Hz.

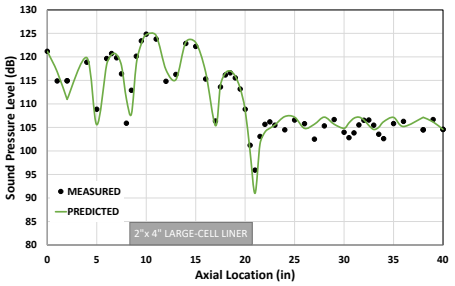

(i) 2” x 4” large-cell liner, 2000 Hz.

Figure 10: Comparison between measured and predicted SPL axial profiles at Mach 0, 120 dB.

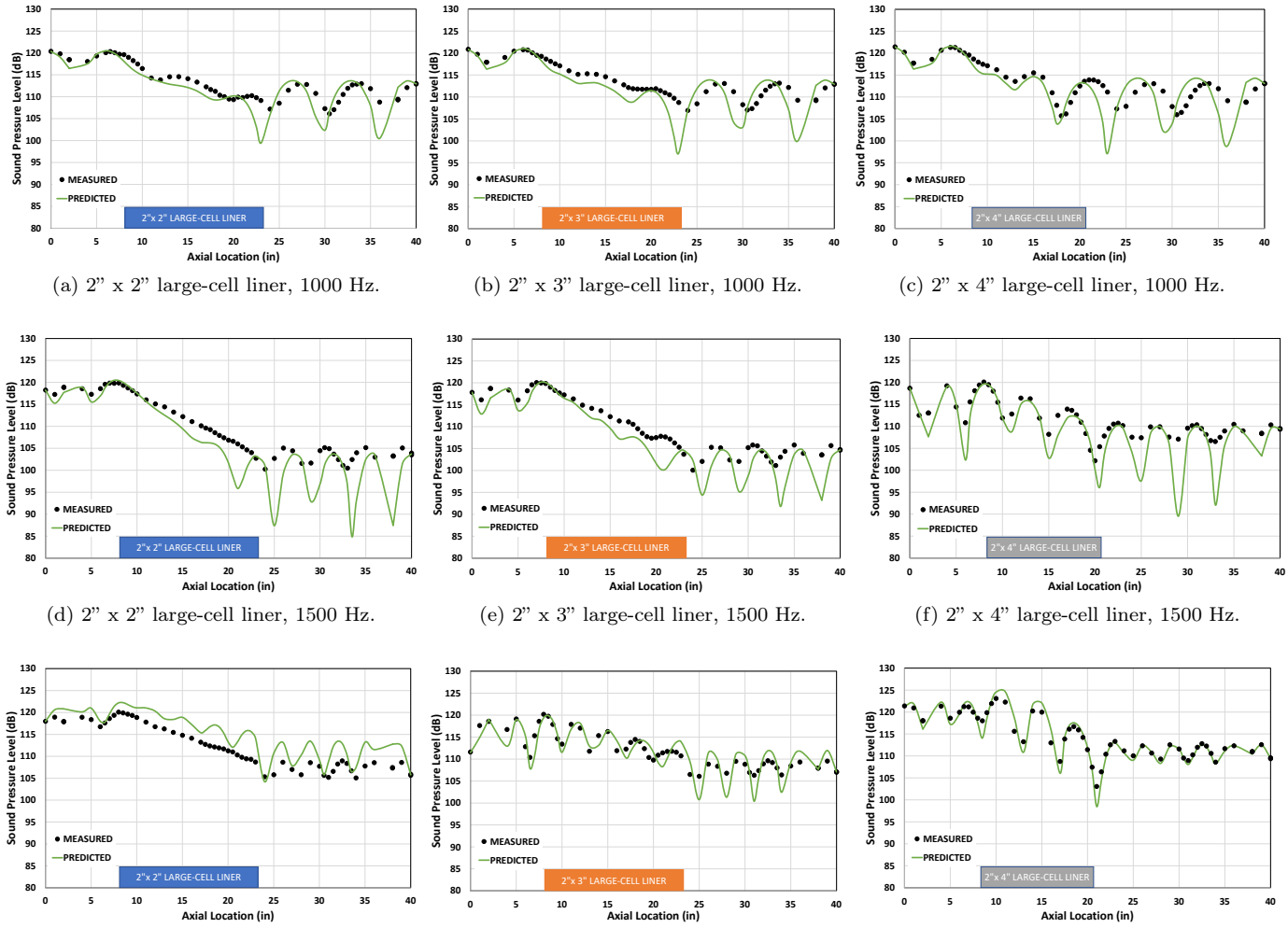

(a) 2” x 2” large-cell liner, 1000 Hz. (b) 2” x 3” large-cell liner, 1000 Hz. (c) 2” x 4” large-cell liner, 1000 Hz.

(d) 2” x 2” large-cell liner, 1500 Hz. (e) 2” x 3” large-cell liner, 1500 Hz. (f) 2” x 4” large-cell liner, 1500 Hz.

(g) 2” x 2” large-cell liner, 2000 Hz. (h) 2” x 3” large-cell liner, 2000 Hz. (i) 2” x 4” large-cell liner, 2000 Hz.

Figure 11: Comparison between measured and predicted SPL axial profiles over length of GFIT test section for large-cell liners at Mach 0.3, 120 dB.

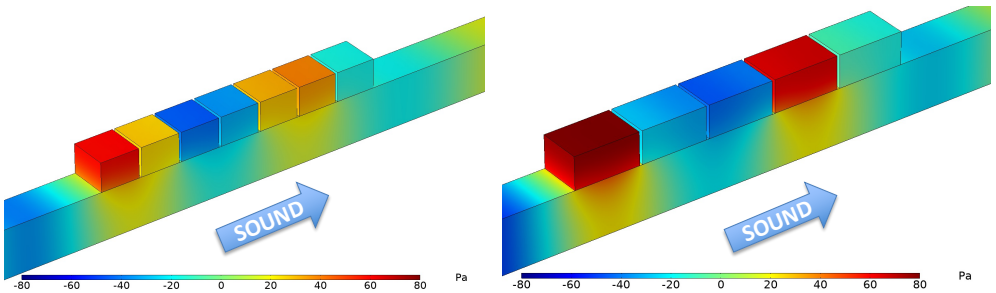

(a) 2” x 2” large-cell liner. (b) 2”x3” large-cell liner.

Figure 12: Real Component of acoustic pressure for a 2” x 2” large-cell liner and 2” x 3” large-cell liners at Mach 0, 120 dB, 1000 Hz.

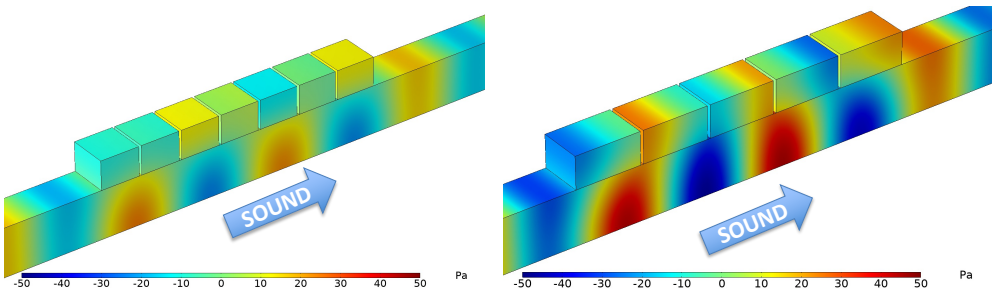

(a) 2"x2" large-cell liner. (b) 2"x3" large-cell liner.

Figure 13: Real Component of acoustic pressure for a 2" x 2" large-cell liner and 2" x 3" large-cell liner at Mach 0, 120 dB, 2000 Hz.

VI. Concluding Remarks

The goal of this study was to explore the effects of increasing the cell size for large-cell acoustic liners. Three samples with cell dimensions of 2" x 2", 2" x 3", and 2" x 4" were fabricated and tested in the NASA Langley Grazing Flow Impedance Tube. Each liner was evaluated using a conventional impedance eduction method intended for use with locally reacting liners. Deviations of the impedances educed for the liners with larger cell dimensions from that educed for the 2" x 2" large-cell liner confirmed that liners with larger cell sizes must be evaluated using nonlocally reacting assumptions. Regardless, all three liners were shown to provide good attenuation. Three methods were explored for the determination of a transfer impedance that could be used in simulations with finite element methods to properly predict the measured sound field for each of these liners. Excellent comparisons of measured and predicted sound pressure level axial profiles were achieved using this approach, thereby confirming the ability to use this approach for modeling large-cell liners. Similar to earlier studies for liners with smaller (up to 2" x 2") cell dimensions, future studies will focus on evaluating the efficacy of the current prediction approach for use in more complex aeroacoustic environments. Specifically, samples with larger cell dimensions will be tested in the NASA Langley Curved Duct Test Rig, where the acoustic source consists of controlled higher-order modes.

Acknowledgments

The authors would like to thank the following people who were instrumental to the success of this investigation: Mr. Alonzo (Max) Reid in the Aeroacoustics Branch for outstanding testing support, Mr. Christopher (Mark) Cagle in the Aeronautics Systems Engineering Branch for outstanding support in designing the samples, and Mr. Robert C. Andrews in the Manufacturing Applications Branch for outstanding 3D printing services. This work was funded by the Advanced Air Transport Technology Project of the NASA Advanced Air Vehicles Program.

References

[1]Ingard, U. and Labate, S., "Acoustic Circulation Effects and the Nonlinear Impedance of Orifices," *The Journal of the Acoustical Society of America*, Vol. 22, No. 2, 1950, pp. 211–218.

[2]Brown, M. C. and Jones, M. G., "Effects of Cavity Diameter on Acoustic Impedance of Perforate-Over-Honeycomb Liners," AIAA Paper 2017-4189, 23rd AIAA/CEAS Aeroacoustics Conference, Denver, Colorado, June 2017.

[3]Brown, M. C. and Jones, M. G., "Effects of Cavity Diameter on Acoustic Impedance in a Complex Acoustic Environment," AIAA Paper 2018-3443, 24th AIAA/CEAS Aeroacoustics Conference, Atlanta, Georgia, June 2018.

[4]Gravagnone, N., Murray, P., and Di Giulio, M., "Optimisation of non-locally reacting liners for improved duct attenuation," AIAA Paper 2022-2931, 28th AIAA/CEAS Aeroacoustics Conference, Southampton, United Kingdom, June 2022.

[5]*COMSOL Multiphysics Reference Manual, version 6.0, COMSOL, Inc.*, www.comsol.com.

[6]Bendat, J. S. and Piersol, A. G., *Random Data: Analysis and Measurement Procedures*, Wiley-Interscience, 1971.

[7]de Prony, R., "Essai Éxperimental et Analytique: Sur Les Lois de la Dilatabilité de Fluides Élastique et sur Celles de la Force Expansive de la Vapeur de L'alkool, Àdifférentes Temperatures," *Journal de l'école Polytechnique*, Vol. 1, No. 22, 1795, pp. 24–76.

[8]Watson, W. R., Carpenter, M. H., and Jones, M. G., "Performance of Kumaresan and Tufts Algorithm in Liner Impedance Eduction with Flow," *AIAA Journal*, Vol. 53, No. 4, April 2015, pp. 1091–1102.

[9]*Actran 2022 User's Guide Vol. 1 – Installation, Operations, Theory, and Utilities*, 2022.

[10]Parrott, T. L. and Jones, M. G., "Assessment of NASA's Aircraft Noise Prediction Capability, Chapter 6: Uncertainty in Acoustic Liner Impedance Measurement and Prediction," NASA TP 2012-215653, July 2012.

[11]Yu, J., Ruiz, M., and Kwan, H. W., "Validation of Goodrich Perforate Liner Impedance Model Using NASA Langley Test Data," AIAA Paper 2008-2930, 14th AIAA/CEAS Aeroacoustics Conference, Vancouver, British Columbia, May 2008.

[12]Jones, M. G., Watson, W. R., and Nark, D. M., "Effects of Flow Profile on Educed Acoustic Liner Impedance," AIAA Paper 2010-3763, 16th AIAA/CEAS Aeroacoustics Conference, Stockholm, Sweden, June 2010.

[13]Myers, M. K., "On the Acoustic Boundary Condition in the Presence of Flow," *Journal of Sound and Vibration*, Vol. 71, No. 3, 1980, pp. 429–434.

[14]Watson, W. R. and Jones, M. G., "A Comparative Study of Four Impedance Eduction Methodologies Using Several Test Liners," AIAA Paper 2013-2274, 19th AIAA/CEAS Aeroacoustics Conference, Berlin, Germany, May 2013.